ACS Electrochemistry

pubs.acs.org/electrochem Article

# Investigation of Noise at a Microelectrode during a Faradaic Reaction

Kaden Wheeler, Joseph Gott, Brian Roehrich, Julia Chung, Kajal Kajal, Jaroslaw Syzdek, Joao Hespanha, and Lior Sepunaru*

Cite This: https://doi.org/10.1021/acselectrochem.4c00117 Read Online

ACCESS | Metrics & More | Article Recommendations | Supporting Information



**ABSTRACT:** Measurement of small currents is often impeded by a suboptimal signal-to-noise ratio, largely due to background noise. This background noise significantly constrains the range of catalysts accessible for interrogation via micro- and nanoscale electrochemistry. In response, this work reveals how background noise scales in the presence of induced Faradaic reactions. We measured noise under a series of electrochemical conditions and discovered that the induced noise from a Faradaic reaction scales directly with current. Complementary electrochemical impedance spectroscopy measurements demonstrated that diffusional resistance dictates the noise of Faradaic reactions, independent of the electrochemical mechanism. The noise source is thermal in origin and propagates in a predictable trend, which is inversely proportional to the equivalent diffusional resistance of the analyte. The universality of the observed phenomenon allows for better deconvolution of measured charge from background noise, thus assisting in achieving higher resolution and measurement precision, which is a key in micro- and nanoscale electrochemical measurements.

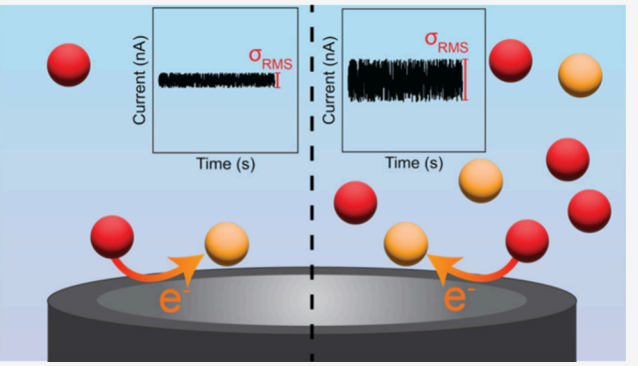


**KEYWORDS:** *microelectrode, Faradaic reaction, electrochemical noise, diffusion, shot noise, thermal noise*

## INTRODUCTION

Micro- and nanoscale electrochemistry requires low-noise instrumentation to measure small currents on the scale of picoamps or femtoamps.[1−5] While picoamp currents are readily resolved in corrosion,[6,7] biosensors,[8] and nanoparticle catalysis,[3] smaller currents are masked by background electrochemical noise.[9,10] Specifically, there are few instances[11] where single molecular catalysts and individual enzymes are measurable with electrochemical methods. In most cases, the inherent heterogeneity in size and activity of these systems is obscured by low signal-to-noise ratios.[12−16] A better understanding of electrochemical noise can help deconvolute the signal from the noise, extending detection limits and broadening the range of measurable catalysts, especially those limited by sluggish kinetics rather than diffusion.

Five common noise sources need to be considered in any electrochemical measurement: mechanical, electromagnetic, flicker, thermal, and shot noise.[17] Electromagnetic noise, also considered as electromagnetic interference, is caused by incident electromagnetic waves, often originating from electrical mains and thus inducing 50 or 60 Hz noise (depending on the local mains frequency). By using nested Faraday cages, electromagnetic noise is minimized to the extent that it does not affect measurements.[18] Mechanical noise originates from physical vibrations during a measurement, for example, while using a rotating disk electrode. However, mechanical noise is substantially attenuated when using a properly insulated stationary electrode, as in this work. Flicker noise, also coined pink noise or $1/f$ noise, is an additional low frequency noise source that aptly scales inversely with frequency.[19,20] In this work, flicker noise is not considered since we have no detectable $1/f$ trends. Because of these reasons, hereafter we consider shot and thermal noise, which are unavoidable in any electrochemical system.[21,22]

Shot noise stems from random fluctuations in the number of electrons passing through the electrode due to the discrete charge of electrons.[23,24] Shot noise is described by eq 1, where $\sigma_i$ is the root-mean square (RMS) current noise, $q_e$ is the charge of an electron, $i$ is the measured current, and $f$ is the bandwidth of the measurement, the maximum observable frequency.[25,26] This predicts that baseline current noise will scale proportionally with the square root of current.

**Received:** October 3, 2024
**Revised:** February 6, 2025
**Accepted:** February 12, 2025

$$\sigma_i = \sqrt{2q_e if} \quad (1)$$

Thermal noise, also called Johnson−Nyquist noise, arises from vibrations of charge carriers in conductors, and is classically described by eq 2 where $\sigma_T$ is the RMS current noise, $k_B$ is the Boltzmann constant, $T$ is the temperature of the cell, and $R$ is the resistance through which current is passed.[27,28]

$$\sigma_T = \sqrt{\frac{4k_B Tf}{R}} \quad (2)$$

The differences in how shot noise and thermal noise scale make it straightforward to distinguish between them in a simple system like a resistor. Thermal noise depends on the resistor's impedance, while shot noise depends on the current. By varying the potential over a sufficiently wide range, the relative contributions of shot and thermal noise to the total current noise can be determined.

Previous work shows that noise at an electrode surface doing no catalysis is thermal in origin,[29−31] while shot noise has been suggested as the limiting factor in single-entity measurements.[10] Further works have characterized shot noise in redox monolayers[32] as well as derived theoretical results for electrolyte effects on measured noise.[33] In this study, we quantify and categorize noise in the presence of an induced Faradaic reaction, similar to background reactions caused by dissolved atmospheric species or any undesired redox reaction occurring at an electrode surface. Since a working electrode is not perfectly inert, it will undergo some Faradaic processes that contribute to the background current in a real electrochemical cell. By coupling chronoamperometric measurements with impedimetric measurements, we demonstrate that the dominant source of noise amid background reactions at the microscale is thermal in origin and dictated by the diffusional resistance of the redox probe. However, the measured noise resulting from this resistance does not trend with the inverse square root of resistance as predicted by the Johnson−Nyquist equation; rather the noise is inversely proportional to the equivalent diffusional resistance.

## EXPERIMENTAL SECTION

**Instrumentation and Equipment.** Common redox probes were used as a model system to mimic the presence of a background reaction. $[Ru(NH_3)_6Cl_3]$ (Sigma-Aldrich, 98%), 2,2,6,6-tetramethyl-1-piperidinyloxyl (TEMPO, Oakwood Chemicals, 99%), maltose (Sigma-Aldrich, ≥99%), KCl (Sigma-Aldrich, 99.0-100.5%), sodium bicarbonate (Fisher Chemical, 99.7-100.3%), and sodium carbonate (Fisher Chemical, 99.9%) were purchased and used as received. $[Ru(NH_3)_6Cl_3]$ solutions were prepared with aqueous 1 M [KCl] as supporting electrolyte, unless stated otherwise, and sparged with Ar gas. TEMPO solutions were prepared in 50 mM sodium carbonate−sodium bicarbonate buffer solution at pH = 10.25.[34]

All measurements were recorded on a Biologic SP-300 with an ultra-low current probe. A 50 kHz 4-pole analog low-pass filter was applied, and the systems were recorded on a bandwidth of 8 as defined by the manufacturer (160 kHz unity gain). The potentiostat employs a 25 kHz sampling rate which was further averaged to a final reported frequency of 1 kHz. The frequency averaging has the expected relation of square root of $f$ with noise (Figure S1). Due to an initial sampling rate at a high frequency of 25 kHz, the effect of aliasing on the measured current noise is mitigated (see note following Figure S1). The working electrode is a 5.5 $\mu$m radius carbon fiber ultramicroelectrode purchased from BASI. All wet electrochemistry experiments were run in a three-electrode configuration. A platinum wire was used as the counter electrode and a saturated calomel electrode was used as the reference electrode. Both the counter and the reference electrode were purchased from CH Instruments. All electrodes are placed into a single glass vial with no dividers. The carbon fiber working electrode was polished before every set of experiments and between each individual TEMPO measurement.

**Determination of Noise in Resistors.** Root-mean-square noise at the varying resistors was calculated via eqs 4 and 5 from measured chronoamperometry experiments. Resistors used were measured via electrochemical impedance spectroscopy to be 0.67, 1.03, 2.23, 8.15, and 10.50 MΩ. A 100 nA current range and a bandwidth of 8, as defined by the manufacturer, were used in the measurement to be comparable to the chemical measurements. The potentiostat was used in the three-electrode configuration with the reference electrode connection connected with the counter electrode connections. Potential dependent measurements were taken at the 1.03 MΩ while varying potential from 1 mV to 145 mV in a 2 min measurement, while resistance dependent measurements were taken across all resistors at 100 mV in a 2 min measurement.

**Determination of Noise in Chemical Systems.** A 10 nA current range was used to record all the TEMPO data, while the $[Ru(NH_3)_6Cl_3]$ data was measured in the 100 nA current range. The differences in the current range are due to the concentration ranges used in the experiments. TEMPO has a limited concentration range due to low solubility in aqueous solution, thus TEMPO was measured in a concentration range from 0−10 mM. Meanwhile $[Ru(NH_3)_6Cl_3]$ has higher solubilities in aqueous solutions, so $[Ru(NH_3)_6Cl_3]$ was measured from 0−100 mM.

Root-mean-square noise was calculated via eqs 4 and 5 from measured chronoamperometry experiments. Chronoamperograms were measured at the potential in the diffusion-limited, steady-state current regime of each redox probe to limit the effect of voltage noise (sampled for 2 min). Initial cyclic voltammograms (CVs) of each redox probe (150 mV/s) were taken to determine where the potential in the diffusion-limited, steady-state current regime occurred (0.8 V vs SCE for TEMPO and -0.7 V vs SCE for $[Ru(NH_3)_6Cl_3]$).

**Electrochemical Impedance Spectroscopy.** Potentiostatic Electrochemical Impedance Spectroscopy (EIS) measurements were recorded at the formal redox potentials for each redox probe (0.5 V vs SCE for TEMPO, -0.2 V vs SCE for $[Ru(NH_3)_6Cl_3]$). A 10 mV sinusoidal perturbation was applied with a frequency range from 100 kHz to 100 mHz.

## RESULTS

**Potentiostatic Influences on Current Noise in Resistors.** Before doing any chemical measurements, we recorded current noise across various resistors. According to the Johnson−Nyquist eq (eq 2), the measured current noise should scale inversely with the square root of resistance and be independent of current. On the other hand, shot noise (eq 1) predicts a measured noise that scales proportionally with the square root of the current. However, shot noise is expected to be less than predicted by eq 1 in a simple macroscopic resistive


https://doi.org/10.1021/acselectrochem.4c00117
ACS Electrochem. XXXX, XXX, XXX−XXX

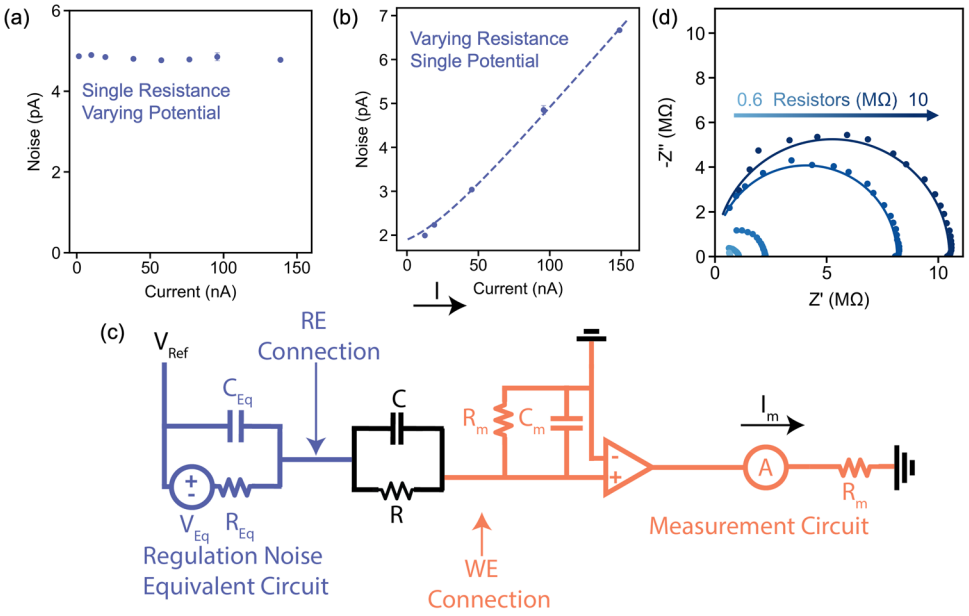


**Figure 1.** Noise at a resistor is dictated by intrinsic thermal noise and potential fluctuations in the regulation circuit within a potentiostat. (a) RMS current noise at the 1.03 MΩ resistor while varying the applied potential from 1−145 mV. (b) RMS current noise at varying resistors, with a constant applied potential, plotted against the derived eq (eq 3, $V_{App}$ = 0.1 V, $R_{Res}$ = 0.67, 1.03, 2.23, 8.15, 10.50 MΩ, $R^2$ = 0.998). (c) The equivalent circuit of the resistor (black) and its connections to the potentiostat, the regulation circuit (blue) and the working electrode connection (orange), without considering the counter electrode connection. (d) Recorded impedance spectra at resistors of varying resistances (0.67, 1.03, 2.23, 8.15, 10.50 MΩ). Solid lines are fit to an impedance accounting for the regulation noise equivalent circuit, the stray capacitance from the potentiostat, and the resistor itself.

circuit, as well as in circuits where negative feedback acts to quiet shot noise.[35,36] As an initial verification, we measured noise across a constant resistance and varied potential, finding that the measured noise does not change (Figure 1a), a result in line with the predicted Johnson-Nyquist behavior and with the expected minimal shot noise. However, when measuring at a constant potential and varying the resistor, the noise seemed to scale linearly with increasing current (decreasing resistance) (Figure 1b), an unexpected result from the predicted square root trend in eq 2. This linear phenomenon cannot be explained by thermal or shot noise characteristics inherent to the resistor alone as they both scale with a square root trend independently.

The measured current noise results from the combination of two sources: the intrinsic noise of the resistors and the noise induced by potentiostatic voltage fluctuations. For the latter, an ideal potentiostat precisely regulates the reference potential, yet in practice, the reference potential will exhibit some noise superimposed on the desired potential. To determine the effect of the potential fluctuations on the measured noise at the resistors, we considered both the measurement circuit of the potentiostat and an equivalent circuit for controlling the potential of the working electrode. The equivalent circuit consists of one RC loop that allows a derivation of noise from this circuit (eq 3, Tables S1−S2). The derivation of this equation assumes that the two noise sources act independently and thus can be superimposed (see Derivation of Equation 3 in the SI). In this equation, $R$ is the measured resistance, $C$ is the stray capacitance (Figure 1c, black), and $\psi$ is a white noise voltage source with a constant power spectral density.[37] Further, $R_{eq}$ and $C_{eq}$ are the equivalent impedances of the potentiostat regulation circuitry (Figure 1c, blue), while $R_m$ and $C_m$ are the equivalent impedances of the measurement circuit (Figure 1c, orange). To determine the impedance of the resistance and stray capacitance (Figure 1c, black), we can fit the Nyquist plots in Figure 1d to the equivalent RC circuit (Table S1). The equivalent impedances of the measurement and regulation equivalent circuits are estimated for a commercial potentiostat (Table S2).[38,39] eq 3 then describes the expected RMS current noise at varying resistances. This equation is a ratio of quadratic expressions in R (see Table S2 for the parameters used and further calculation), which becomes linear with respect to the current (inverse of R) in the regime we are observing. Fitting of eq 3 to our experimental data produces a high linear correlation ($R^2$ = 0.995, dashed line in Figure 1b). We conclude that the unexpected linear correlation between the current noise and the total current measured is caused by the equivalent regulation circuit and the thermal noise stemming from the resistor itself.

$$\sigma_{Res} = \sqrt{\frac{k_B T \frac{R}{R^{\perp}}\left(\frac{R_{eq}C_{eq}R^{\perp}C^{\perp}}{RCR_mC_m} + 1\right) + \frac{1}{2}\left(\frac{RCR^{\perp}C^{\perp}}{R_{eq}C_{eq}R_mC_m} + 1\right)\frac{\psi^2}{R^{\perp}}}{(R + R_m)R_{eq}C_{eq} + (R_{eq} + R_m)RC + (R + R_{eq})R_mC_m}} \quad (3)$$

where

$$R^{\perp} := R + R_{eq} + R_m \qquad C^{\perp} := \frac{CC_mC_{eq}}{CC_{eq} + CC_m + C_mC_{eq}}$$

**Electrochemical Noise during Heterogeneous Redox Reactions.** After understanding the potentiostat's effect on noise, we investigated our initial question of how current noise scales with a background Faradaic reaction at a microelectrode. To measure changes in current noise driven by Faradaic reactions, we used Tetramethylpiperidine N-Oxyl (TEMPO)


https://doi.org/10.1021/acselectrochem.4c00117
ACS Electrochem. XXXX, XXX, XXX−XXX

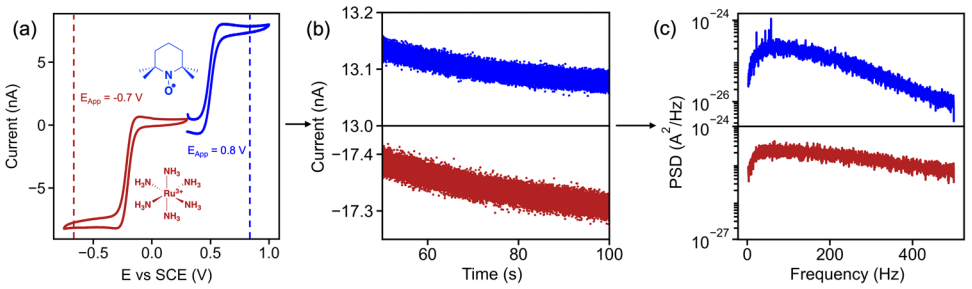


**Figure 2.** Noise in the diffusion-limited, steady-state current regime of an induced Faradaic reaction is frequency independent, indicating its source to be fundamentally shot or thermal noise. (a) Cyclic voltammograms of $[Ru(NH_3)_6Cl_3]$ (red, 5 mM $[Ru(NH_3)_6Cl_3]$, 1 M [KCl], sparged with Ar gas) and TEMPO (blue, 5 mM TEMPO, 50 mM sodium carbonate−sodium bicarbonate buffer) (150 mV/s). The observed redox couple in blue at 0.503 V vs SCE corresponds to the TEMPO/TEMPO$^+$ couple. (b) Chronoamperograms at potentials in the diffusion-limited, steady-state current regime (-0.7 V vs SCE for 10 mM $[Ru(NH_3)_6Cl_3]$, 10 mM [KCl], sparged with $N_2$ gas; 0.8 V vs SCE for 5 mM TEMPO, 50 mM sodium carbonate−sodium bicarbonate buffer, 1000 Hz sampling frequency) of both species allowing for the (c) calculated power spectral densities (PSD, 10 mM $[Ru(NH_3)_6Cl_3]$, 10 mM [KCl], sparged with $N_2$ gas; 10 mM TEMPO, 50 mM sodium carbonate−sodium bicarbonate buffer).

and Hexaammineruthenium(III) chloride ($[Ru(NH_3)_6Cl_3]$) as the redox probes because they have well-known electrochemical behavior. $[Ru(NH_3)_6Cl_3]$ ($D_{[Ru(NH_3)_6Cl_3]}$ = (7.41 ± 0.36) × $10^{-6}$ $cm^2/s$, Figure S2, Table S3)[40] is an outer-sphere electrochemical redox probe,[41,42] while TEMPO ($D_{TEMPO}$ = (8.08 ± 0.08) × $10^{-6}$ $cm^2/s$, Figure S2, Table S4)[43] has a more complex proton-coupled electrochemical mechanism.[34] As a first verification for the validity of our measurements, our measured diffusion coefficients are comparable to literatures. The variety in electrochemical mechanisms may allow for the following results to be generalizable to any background Faradaic reaction with freely diffusing redox probes. By increasing the concentration of the redox probe in solution, the flux of the redox probe towards the electrode surface will increase. An increased flux leads to an increase in the induced current, and thus the induced current noise will increase which can be measured via chronoamperometry. Potentials in the diffusion-limited, steady-state current regime of each redox probe were chosen for the chronoamperometry experiments to ensure that fluctuations in the applied potential were negligible in the measurement of current and current noise. Cyclic voltammograms of each redox probe (Figure 2a) showed that the formal potential of $[Ru(NH_3)_6Cl_3]$ was -0.205 V vs SCE and that the formal potential of TEMPO was 0.503 V vs SCE, which were similar to literature values.[44,45] The applied potentials in the diffusion-limited, steady-state current regime were more than 300 mV away from the formal potentials, guaranteeing that the measurement is within the diffusion-limited regime.

Next, we measured chronoamperograms at the potentials in the diffusion-limited, steady-state current regime to calculate noise. We first verified that the noise in the measured chronoamperograms was random with no outliers (Figure 2b). To calculate the RMS current noise from the chronoamperogram, the power spectral density (PSD) of the chronoamperogram is calculated first using Welch's method (eq 4). The Welch method was used to determine noise in order to account for any nonlinearity contributions that the time-domain definition of RMS noise may not have accounted for. Time domain data is partitioned into equal length segments, discrete Fourier transformed, squared, and averaged to calculate the PSD. A simplified view of Welch's discrete method is shown in eq 4, where $P_k$ is the $k^{th}$ modified periodogram and $K$ is the total number of periodograms, which is analogous to calculating the PSD of continuous data.[46−48]

The DC component of the measurement was eliminated by sampling the PSD above 1 Hz. The lack of signal seen around 60 Hz in the PSD shows that electromagnetic noise is minimized via the experimental setup, verifying that the noise is not dominated by an electromagnetic phenomenon.[18] Further, we observed that the noise is relatively frequency-independent (varying by less than two orders of magnitude, Figure 2c), as expected for shot or thermal noise.[25,27,28] Finally, root-mean-square noise was calculated by integrating the PSD (eq 5).[29,46] Values for the RMS noise obtained this way align well with those measured directly from chronoamperograms in the time domain (Figure S3).

$$\mathrm{PSD} = \frac{1}{K}\sum_{k=1}^{K} P_k(f) \approx \frac{\left(\int_{-\infty}^{\infty} f(t)e^{-j\omega t}\,dt\right)^2}{2f} \tag{4}$$

$$\sigma_{RMS} = \sqrt{\sum \mathrm{PSD}(f)\Delta f} \tag{5}$$

We measured chronoamperograms across a range of redox probe concentrations to test the scaling relationship between noise and current. TEMPO is limited to a narrow concentration range (0−10 mM) because of low solubility in aqueous solutions. This low solubility limits the measurable range of currents (Figure 3b, blue), but within this range, we found that noise scales linearly with current. This linear scaling holds true when switching to a redox probe with higher solubility, $[Ru(NH_3)_6Cl_3]$ (0−100 mM, Figure 3a, red). We note that the electrochemical current noise is invariant of electrolyte concentration (Figure S4). At first glance, this is not surprising since the measurement of a resistor's noise also scales linearly with current. In the case of the resistors, this deviation was attributed to potential fluctuations of the voltage control circuit−however, in the diffusion-limited, steady-state regime of this electrochemical measurement, current is independent of potential, thus the potential fluctuations should not affect the current noise. Further, to evaluate the baseline noise and how the noise propagates, we fit the data to a linear model. The y-intercepts of the linear fits characterize the baseline noise from the potentiostat. In both cases, the baseline noise is on the order of 1 pA. Interestingly, the slope of each probe is statistically different, which could be caused by differences in the redox probes' diffusion coefficients or exchange current densities. In addition, when the temperature


https://doi.org/10.1021/acselectrochem.4c00117
ACS Electrochem. XXXX, XXX, XXX−XXX

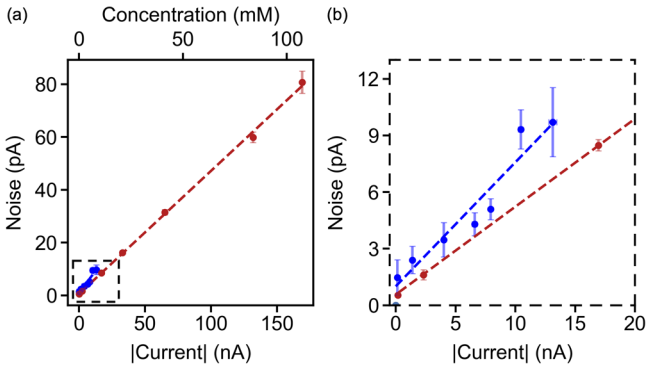


**Figure 3.** Faradaic noise scales linearly with current at a microelectrode regardless of redox probe. (a) RMS current noise (pA) vs current (nA) of $[Ru(NH_3)_6Cl_3]$ (red, 0−100 mM $[Ru(NH_3)_6Cl_3]$, 10 mM [KCl]) across a wide range of currents showing linearity. (b) Comparing the RMS current noise (pA) vs current (nA) of two redox probes, $[Ru(NH_3)_6Cl_3]$ (red, 0−10 mM $[Ru(NH_3)_6Cl_3]$, 10 mM [KCl], sparged with Ar gas) and TEMPO (blue, 0−10 mM TEMPO, 50 mM sodium carbonate−sodium bicarbonate buffer), showing linearity for both probes. (Data fit to $y = mx + b$; $[Ru(NH_3)_6Cl_3]$ fit line parameters: $|m| = (4.67 \pm 0.070) \times 10^{-4}$, $b = 0.58 \pm 0.62$ pA, $R^2 = 0.999$. TEMPO fit line parameters: $m = (6.63 \pm 0.89) \times 10^{-4}$, $b = 0.99 \pm 0.66$ pA, $R^2 = 0.917$).

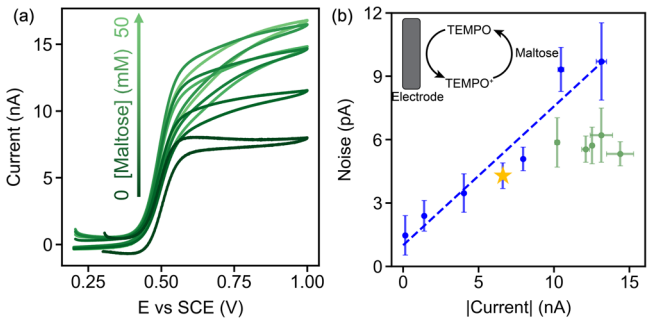


**Figure 4.** Noise stays constant while the absolute current increases during an electrocatalytic coupled reaction. (a) TEMPO CVs with increasing maltose concentration (5 mM TEMPO, 0−50 mM maltose, 50 mM sodium carbonate−sodium bicarbonate buffer). (b) RMS noise (pA) vs current (nA) for the maltose amplified TEMPO system (5 mM TEMPO, 0−50 mM maltose, 50 mM sodium carbonate−sodium bicarbonate buffer). The star is 0 mM maltose, and the green points correspond to 10−50 mM maltose. The data is plotted against the linear fit for the TEMPO without maltose system (dashed, blue line) along with the original TEMPO data without maltose (blue). The mechanism scheme is shown with the inset.

of the system is raised by $\Delta T = 35$ K, the current noise is increased by 5% (Figure S5, $T_1 = 298$ K, $T_2 = 333$ K). The thermal noise described in eq 2 predicts that the noise will vary by about 6%, in line with our experimental observation. However, under aqueous conditions, using temperature as a direct parameter for deciphering the origins of noise is limited to only a narrow range of temperatures and can cause further complications. For example, by raising the temperature further in an aqueous solution, the analyte concentration will change due to evaporation, as well as changing viscosity and diffusion coefficients. Similarly, temperature and concentration gradients can lead to natural convection at the electrode surface, a phenomenon that has been shown to have potentially large effects on the measured current in systems with larger ultramicroelectrodes (radii larger than about 10 $\mu$m). However, in this work, the small dimensions of the ultramicroelectrode (with a radius of 5.5 $\mu$m), combined with the relatively short measurement time, negate the influence of natural convection on the measured noise.[49,50] Nonetheless, shot noise requires the measured current noise to scale with the square root of current (eq 1) and the lack of this trend suggests that our noise is not dictated by shot noise.

**Faradaic Noise during an Electrocatalytic Reaction (EC′).** As we observed an unexpected result of the RMS current noise scaling linearly with Faradaic current, we next switched the reaction mechanism from a strictly electrochemical mechanism to a chemically amplified electrocatalytic system (EC′) to further validate if this result is generalizable. An EC′ mechanism introduces a chemical species, maltose in this work, which increases the observed current.[51,52] This increased current can be directly observed in cyclic voltammetry experiments with 5 mM TEMPO (Figure 4a). Specifically, maltose locally reduces $TEMPO^+$, increasing the flux of TEMPO to the surface, resulting in current amplification (Figure 4b inset).[34,44] As the concentration of maltose increases, the measured current from the oxidation of TEMPO increases before plateauing at high maltose concentrations.[53] However, the measured noise in these conditions stayed constant at increasing maltose concentrations (Figure 4b). This trend becomes apparent when plotting the amplified system's noise against the fit of the TEMPO alone system from Figure 3b (blue, dashed line in Figure 4b). The noise observed at every data point in the TEMPO-maltose system (green) is significantly lower than the noise expected from the fitted TEMPO alone system (blue) across all maltose concentrations. Moreover, no clear trend is observed between noise and the theoretical predictions for current, where current scales with the square root of the mediator concentration for an EC′ reaction (Figure S6).[44,53] To validate this phenomenon is not limited to the lower bounds of our measured currents, we repeated the experiment at higher currents by increasing the concentration of TEMPO (Figure S7). In this case, the measured noise remains significantly lower than that predicted by the TEMPO alone system and seems independent of the measured steady state current. This result eliminates shot noise as the dominant source of noise and suggests that a thermal phenomenon is dictating the measured noise during the induced Faradaic reactions.

**Electrochemical Impedance Reveals the Dominant Noise Source Is Diffusional Resistance.** Our empirical results exceed the combined contributions of classical shot and thermal noise (eqs 1 and 2, Figure S8). To further understand these deviations, we sought to determine the equivalent circuit component in our electrochemical cell which dictates the current noise. Here, we remind the reader that in an electrochemical system, the equivalent impedances are no longer purely real as in eq 2. Specifically, a microelectrode undergoing a Faradaic reaction contains multiple imaginary impedances: one arising from the double layer and the other from the behavior of redox probe diffusion (Figure S9 (a) inset for the common circuit diagram of a microelectrode).[54−57] This common microelectrode circuit diagram accounts for: $R_{Sol}$, the solution resistance; $R_{CT}$, the charge transfer resistance; $C_{DL}$, the double layer capacitance; $R_{Diff}$, a diffusional resistance; $Q_{Diff}$, a constant phase element representing the Warburg impedance. Further, additional stray capacitance may be generated from the potentiostat.[58,59] We propose that the


https://doi.org/10.1021/acselectrochem.4c00117
ACS Electrochem. XXXX, XXX, XXX−XXX

presence of these elements will cause the noise through the electrochemical cell to propagate similarly to noise through a series RC circuit. A capacitor in parallel with the resistor acts as a low-pass filter, leading to the so-called "kTC" noise.[60] Rather than flat across the frequency spectrum, kTC noise has a bandwidth $\Delta f = 1/(2\pi RC)$ determined by the RC loop. In the common microelectrode circuit, this effect arises both in the parallel $Q_{Diff}/R_{Diff}$ (since $Q_{Diff}$ has a capacitive effect) as well as the parallel $C_{DL}/R_{CT}$ (inset in Figure S9 (a)). Regardless of which of the kTC noises dominates, the net effect will be a measured current across $R_{sol}$ and/or $R_{CT}$ with an RMS value that is proportional to $\sqrt{k_B T/(C_{DL})}$ and/or $\sqrt{k_B T/(C_{Diff})}$ and inversely proportional to $R_{sol}$ and/or $R_{CT}$, respectively. The key observation here is that the thermal noise is generated by a resistor in parallel with a capacitor that masks the dependence of the noise on the resistance of that resistor. However, if we measure the current across a second resistor in series with such an RC loop, we will observe noise that is inversely proportional to the resistance of that resistor (purely by Ohm's law). The RC-circuit modified Johnson-Nyquist noise eq (eq 6) predicts no dependence on the frequency of the measurement, an inverse square root dependence on the capacitance of our cell, and an inversely linear dependence on the resistance.[61,62]

$$\sigma_T = \sqrt{\frac{k_B T}{2\pi C R^2}} \tag{6}$$

We directly tested this relationship by measuring the impedance using electrochemical impedance spectroscopy (EIS). While the impedance spectrum of a microelectrode usually contains two arcs, we only observe one in our measurements. This is because the first arc, corresponding to the charge transfer and the double layer, is small and should appear at very high frequency due to fast charge transfer kinetics.[56,63−65] We can recover this feature by lowering the analyte concentration, thus lowering the electron transfer rate (Figure S9, Tables S5−S7). The modified circuit (Figure 5a inset) instead accounts for: $R_{Sol}$, the solution resistance; $R_{Diff}$, a diffusional resistance; $Q_{Diff}$, a constant phase element representing the Warburg impedance. This model accounts for linear diffusion on short time scales (Warburg) and a diffusional equilibrium, which behaves as a resistance, occurring at longer time scales.[66] The measured solution resistances are negligible in comparison to $R_{Diff}$ thus the solution resistances have minimal impact on the equivalent circuit fitting and the origins of the source of noise. Further, the measured noise does not depend on the concentration of electrolyte used, validating that the capacitive noise predicted by eq 6 from the double layer is minimal (Figure S4). The impedances for $Q_{Diff}$ are relatively large compared to that of the stray capacitance of the potentiostat showing that this is an electrochemical phenomenon (Figure 1d, Table S1), which is not dictated by the potentiostat circuitry.

We measured impedance spectra across a range of $[Ru(NH_3)_6Cl_3]$, TEMPO, and TEMPO-Maltose concentrations to test the relationship between resistance and noise. At low redox probe concentrations (Figures 5a and 5b), higher impedances are observed as there are less species in solution diffusing leading to an increased resistance, or impedance, to diffusion. As the redox probe concentration is increased, there is more mass transport to the electrode surface, and the impedance decreases. Consistent with the previous results from the EC′ system, as the current is increased with maltose

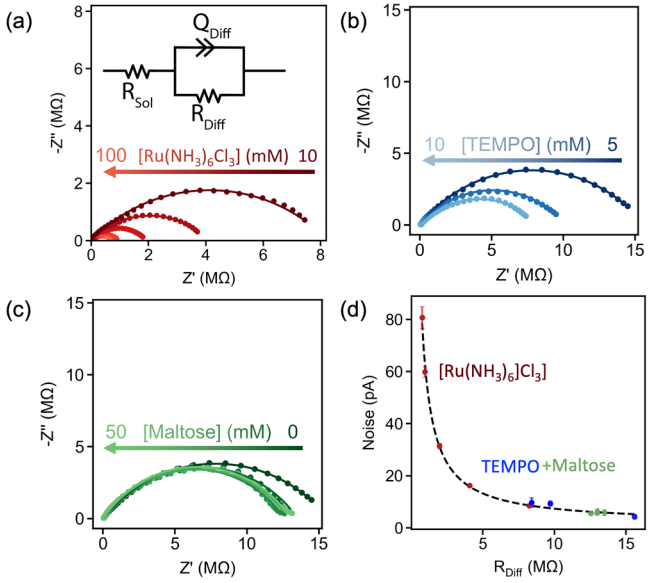


**Figure 5.** Diffusional resistance dictates the noise during background Faradaic reactions at the microscale, independent of the electrochemical mechanism. (a) Nyquist plot of varying concentrations of $[Ru(NH_3)_6Cl_3]$ along with the equivalent circuit (10, 20, 40, 80, and 100 mM $[Ru(NH_3)_6Cl_3]$; 1 M [KCl]; sparged with Ar gas). The experiment was repeated in (b) with the TEMPO alone system (5, 8, and 10 mM TEMPO; 50 mM sodium carbonate−sodium bicarbonate buffer) and in (c) with an electrocatalytic (EC′) mechanism using TEMPO/Maltose system (5 mM TEMPO; 10, 20, 30, 40, and 50 mM maltose; 50 mM sodium carbonate−sodium bicarbonate buffer). (d) The noise is shown to increase as the diffusional resistance decreases and stays constant as the diffusional resistance stays constant. The fit parameters for diffusional resistance (MΩ) were plotted against the RMS noise (pA) in (d). (Data fit to y = m/x +b; Fit line parameters: $m$ = 58.6 ± 1.0 μV, $b$ = 1.48 ± 0.48 pA, $R^2$ = 0.997). All EIS measurements were performed with an applied frequency range of 100 kHz to 100 mHz.

concentration, the impedance stays relatively constant as the maltose concentration increases (Figure 5c). When plotting noise versus resistance for all three data sets combined, a strong fit to $1/R_{Diff}$ (eq 6) is observed (Figure 5d, $R^2$ = 0.997). This high correlation to the diffusional resistance indicates that noise at a microelectrode is thermal in nature, and specifically dictated by diffusional processes.

## CONCLUSION

Understanding the origin and magnitude of electrochemical noise is a critical aspect of electrochemistry, particularly for resolving lower detection limits in biosensors, nano-electrochemistry, and corrosion at conductive surfaces. This study advances prior investigations into electrochemical noise by elucidating its propagation during induced Faradaic reactions. Induced Faradaic reactions provide a more realistic depiction of an electrochemical cell where any dissolved atmospheric species or surface contaminations lead to background Faradaic currents. Using power spectral density and impedimetric measurements, we have determined that Faradaic noise is primarily governed by the diffusional resistance of the system and scales linearly with the concentration of redox active species. This linear response deviates from what is predicted in shot noise and Johnson-Nyquist theory because of the presence of imaginary impedances in the electrochemical cell. These imaginary impedances cause the noise to propagate via a


https://doi.org/10.1021/acselectrochem.4c00117
ACS Electrochem. XXXX, XXX, XXX−XXX

similar phenomenon as kTC noise which is observed in RC circuits. Using the results developed in this work, we offer insights into the background noise generated by impurities to inform future studies. This insight holds for oxidative, reductive, and chemically coupled electrochemical reactions. Further, the RMS current noise reaches a plateau at higher diffusional resistances. We anticipate that this work will assist in better deconvolution of signals to background noise under realistic conditions, and by that, achieve lower detection limits of electronic signals, which is crucial across various subfields of electrochemistry.

## ■ ASSOCIATED CONTENT

### Supporting Information

The Supporting Information is available free of charge at https://pubs.acs.org/doi/10.1021/acselectrochem.4c00117.

Derivation of in-text eq 3 and additional figures and tables (PDF)

## ■ AUTHOR INFORMATION


### Corresponding Author

**Lior Sepunaru** − *Department of Chemistry and Biochemistry, University of California at Santa Barbara, Santa Barbara, California 93106, United States;* orcid.org/0000-0002-4716-5035; Email: sepunaru@ucsb.edu

### Authors

**Kaden Wheeler** − *Department of Chemistry and Biochemistry, University of California at Santa Barbara, Santa Barbara, California 93106, United States;* orcid.org/0009-0009-2699-1838

**Joseph Gott** − *Department of Chemistry and Biochemistry, University of California at Santa Barbara, Santa Barbara, California 93106, United States*

**Brian Roehrich** − *Department of Chemistry and Biochemistry, University of California at Santa Barbara, Santa Barbara, California 93106, United States*

**Julia Chung** − *Interdepartmental Program in Biomolecular Science and Engineering, University of California at Santa Barbara, Santa Barbara, California 93106, United States;* orcid.org/0000-0003-0830-0254

**Kajal Kajal** − *Department of Chemistry and Biochemistry, University of California at Santa Barbara, Santa Barbara, California 93106, United States*

**Jaroslaw Syzdek** − *Bio-Logic USA LLC, Knoxville, Tennessee 37923, United States*

**Joao Hespanha** − *Electrical and Computer Engineering Department, University of California at Santa Barbara, Santa Barbara, California 93106, United States*

Complete contact information is available at: https://pubs.acs.org/10.1021/acselectrochem.4c00117


### Notes

The authors declare no competing financial interest.

## ■ ACKNOWLEDGMENTS

This work was partially funded by NIH grant R35GM142920.

## ■ REFERENCES


(1) Oja, S. M.; Fan, Y.; Armstrong, C. M.; Defnet, P.; Zhang, B. Nanoscale Electrochemistry Revisited. *Anal. Chem.* **2016**, *88* (1), 414−430.

(2) Gilboa, T.; Meller, A. Optical Sensing and Analyte Manipulation in Solid-State Nanopores. *Analyst* **2015**, *140* (14), 4733−4747.

(3) Kanokkanchana, K.; Saw, E. N.; Tschulik, K. Nano Impact Electrochemistry: Effects of Electronic Filtering on Peak Height, Duration and Area. *ChemElectroChem.* **2018**, *5* (20), 3000−3005.

(4) Hoeben, F. J. M.; Meijer, F. S.; Dekker, C.; Albracht, S. P. J.; Heering, H. A.; Lemay, S. G. Toward Single-Enzyme Molecule Electrochemistry: [NiFe]-Hydrogenase Protein Film Voltammetry at Nanoelectrodes. *ACS Nano* **2008**, *2* (12), 2497−2504.

(5) Zhong, C.-B.; Ma, H.; Wang, J.-J.; Zhang, L.-L.; Ying, Y.-L.; Wang, R.; Wan, Y.-J.; Long, Y.-T. An Ultra-Low Noise Amplifier Array System for High Throughput Single Entity Analysis. *Faraday Discuss.* **2022**, *233*, 33−43.

(6) Jadhav, N.; Gelling, V. J. Review—The Use of Localized Electrochemical Techniques for Corrosion Studies. *J. Electrochem. Soc.* **2019**, *166* (11), C3461−C3476.

(7) Mena, E.; Veleva, L.; Souto, R. M. Mapping of Local Corrosion Behavior of Zinc in Substitute Ocean Water at Its Initial Stages by SVET. *Int. J. Electrochem. Sci.* **2016**, *11* (6), 5256−5266.

(8) Yang, C.; Huang, Y.; Hassler, B. L.; Worden, R. M.; Mason, A. J. Amperometric Electrochemical Microsystem for a Miniaturized Protein Biosensor Array. *IEEE Trans. Biomed. Circuits Syst.* **2009**, *3* (3), 160−168.

(9) Hietzschold, S.; Walter, A.; Davis, C.; Taylor, A. A.; Sepunaru, L. Does Nitrate Reductase Play a Role in Silver Nanoparticle Synthesis? Evidence for NADPH as the Sole Reducing Agent. *ACS Sustain. Chem. Eng.* **2019**, *7* (9), 8070−8076.

(10) Gao, R.; Edwards, M. A.; Harris, J. M.; White, H. S. Shot Noise Sets the Limit of Quantification in Electrochemical Measurements. *Curr. Opin. Electrochem.* **2020**, *22*, 170−177.

(11) Sekretaryova, A. N.; Vagin, M. Yu.; Turner, A. P. F.; Eriksson, M. Electrocatalytic Currents from Single Enzyme Molecules. *J. Am. Chem. Soc.* **2016**, *138* (8), 2504−2507.

(12) Davis, C.; Wang, S. X.; Sepunaru, L. What Can Electrochemistry Tell Us about Individual Enzymes? *Curr. Opin. Electrochem.* **2021**, *25*, 100643.

(13) Vannoy, K. J.; Ryabykh, A.; Chapoval, A. I.; Dick, J. E. Single Enzyme Electroanalysis. *Analyst* **2021**, *146* (11), 3413−3421.

(14) Suherman, A. L.; Zhao, Z.; Sekretareva, A. From Protein Film to Single-Entity Protein Electrochemistry. *Curr. Opin. Electrochem.* **2024**, *45*, 101532.

(15) Feng, J. Electrochemistry Probed One Molecule at a Time. *Curr. Opin. Electrochem.* **2022**, *34*, 101000.

(16) Ryu, C. H.; Ren, H. Simultaneous Mapping of Electrocatalytic Activity and Selectivity via Hybrid Scanning Electrochemical Probe Microscopy. *Nano Lett.* **2024**, *24* (20), 6112−6116.

(17) Singh, P. S.; Lemay, S. G. Stochastic Processes in Electrochemistry. *Anal. Chem.* **2016**, *88* (10), 5017−5027.

(18) Glasscott, M. W.; Brown, E. W.; Dorsey, K.; Laber, C. H.; Conley, K.; Ray, J. D.; Moores, L. C.; Netchaev, A. Selecting an Optimal Faraday Cage To Minimize Noise in Electrochemical Experiments. *Anal. Chem.* **2022**, *94* (35), 11983−11989.

(19) Schmid, H. Offset, Flicker Noise, and Ways to Deal with Them. In *Circuits at the Nanoscale*; Iniewski, K., Ed.; CRC Press: 2018; pp 95−115. DOI: 10.1201/9781315218762-7.

(20) Mancini, R.; Carter, B. *Op Amps for Everyone*, 3rd ed.; Newnes/Elsevier: 2009.

(21) Loto, C. A. Electrochemical Noise Measurement Technique in Corrosion Research. *Int. J. Electrochem. Sci.* **2012**, *7* (10), 9248−9270.

(22) Blanter, Ya. M.; Büttiker, M. Shot Noise in Mesoscopic Conductors. *Phys. Rep.* **2000**, *336* (1-2), 1−166.

(23) Einstein, A. Über Einen Die Erzeugung Und Verwandlung Des Lichtes Betreffenden Heuristischen Gesichtspunkt. *Ann. Phys.* **1905**, *322* (6), 132−148.

(24) Davisson, C.; Germer, L. H. Diffraction of Electrons by a Crystal of Nickel. *Phys. Rev.* **1927**, *30* (6), 705−740.

(25) Schottky, W. Über Spontane Stromschwankungen in Verschiedenen Elektrizitätsleitern. *Ann. Phys.* **1918**, *362* (23), 541−567.

(26) Beenakker, C. W. J.; Büttiker, M. Suppression of Shot Noise in Metallic Diffusive Conductors. *Phys. Rev. B* **1992**, *46* (3), 1889−1892.
(27) Nyquist, H. Thermal Agitation of Electric Charge in Conductors. *Phys. Rev.* **1928**, *32* (1), 110−113.
(28) Johnson, J. B. Thermal Agitation of Electricity in Conductors. *Phys. Rev.* **1928**, *32* (1), 97−109.
(29) Yao, J.; Gillis, K. D. Quantification of Noise Sources for Amperometric Measurement of Quantal Exocytosis Using Microelectrodes. *Analyst* **2012**, *137* (11), 2674.
(30) Mierzejewski, M.; Steins, H.; Kshirsagar, P.; Jones, P. D. The Noise and Impedance of Microelectrodes. *J. Neural Eng.* **2020**, *17* (5), 052001.
(31) Urbanová, V.; Li, Y.; Vytřas, K.; Yvert, B.; Kuhn, A. Macroporous Microelectrode Arrays for Measurements with Reduced Noise. *J. Electroanal. Chem.* **2011**, *656* (1-2), 91−95.
(32) Grall, S.; Li, S.; Jalabert, L.; Kim, S. H.; Chovin, A.; Demaille, C.; Clément, N. Electrochemical Shot Noise of a Redox Monolayer. *Phys. Rev. Lett.* **2023**, *130* (21), 218001.
(33) Hoang Ngoc Minh, T.; Kim, J.; Pireddu, G.; Chubak, I.; Nair, S.; Rotenberg, B. Electrical Noise in Electrolytes: A Theoretical Perspective. *Faraday Discuss.* **2023**, *246*, 198−224.
(34) Nutting, J. E.; Rafiee, M.; Stahl, S. S. Tetramethylpiperidine *N* -Oxyl (TEMPO), Phthalimide *N* -Oxyl (PINO), and Related *N* -Oxyl Species: Electrochemical Properties and Their Use in Electrocatalytic Reactions. *Chem. Rev.* **2018**, *118* (9), 4834−4885.
(35) Steinbach, A. H.; Martinis, J. M.; Devoret, M. H. Observation of Hot-Electron Shot Noise in a Metallic Resistor. *Phys. Rev. Lett.* **1996**, *76* (20), 3806−3809.
(36) Horowitz, P.; Hill, W. *The Art of Electronics*, 2nd ed.; Cambridge University Press: 1989.
(37) Papoulis, A.; Pillai, S. U. *Probability, Random Variables, and Stochastic Processes*, 3rd ed.; McGraw-Hill: 1991.
(38) Bard, A. J.; Faulkner, L. R. *Electrochemical Methods: Fundamentals and Applications*, 2nd ed.; Wiley: 2001.
(39) *BIO-LOGIC VMP-300-BASED INSTALLATION AND CONFIGURATION MANUAL PDF Download*. ManualsLib. https://www.manualslib.com/manual/1513013/Bio-Logic-Vmp-300-Based.html (accessed 2024-07-25).
(40) Wang, Y.; Limon-Petersen, J. G.; Compton, R. G. Measurement of the Diffusion Coefficients of [Ru(NH3)6]3+ and [Ru(NH3)6]2+ in Aqueous Solution Using Microelectrode Double Potential Step Chronoamperometry. *J. Electroanal. Chem.* **2011**, *652* (1-2), 13−17.
(41) Xiong, L.; Batchelor-McAuley, C.; Ward, K. R.; Downing, C.; Hartshorne, R. S.; Lawrence, N. S.; Compton, R. G. Voltammetry at Graphite Electrodes: The Oxidation of Hexacyanoferrate (II) (Ferrocyanide) Does Not Exhibit Pure Outer-Sphere Electron Transfer Kinetics and Is Sensitive to Pre-Exposure of the Electrode to Organic Solvents. *J. Electroanal. Chem.* **2011**, *661* (1), 144−149.
(42) Chen, P.; McCreery, R. L. Control of Electron Transfer Kinetics at Glassy Carbon Electrodes by Specific Surface Modification. *Anal. Chem.* **1996**, *68* (22), 3958−3965.
(43) Carlson, E. D.; Majda, M. Electrochemistry of TEMPO: An Assessment of the Water Diffusion Constant in the Aqueous Liquid/Vapor Interfacial Region. *J. Solid State Electrochem.* **2013**, *17* (12), 3083−3091.
(44) Chung, J.; Hertler, P.; Plaxco, K. W.; Sepunaru, L. Catalytic Interruption Mitigates Edge Effects in the Characterization of Heterogeneous, Insulating Nanoparticles. *J. Am. Chem. Soc.* **2021**, *143* (45), 18888−18898.
(45) Campos, R.; Ferapontova, E. E. Electrochemistry of Weakly Adsorbed Species: Voltammetric Analysis of Electron Transfer between Gold Electrodes and Ru Hexaamine Electrostatically Interacting with DNA Duplexes. *Electrochimica Acta* **2014**, *126*, 151−157.
(46) Youngworth, R. N.; Gallagher, B. B.; Stamper, B. L.; Stahl, H. P. An Overview of Power Spectral Density (PSD) Calculations. *Proc. SPIE* **2005**, *5869*, 206.
(47) Welch, P. The Use of Fast Fourier Transform for the Estimation of Power Spectra: A Method Based on Time Averaging over Short, Modified Periodograms. *IEEE Trans. Audio Electroacoustics* **1967**, *15* (2), 70−73.
(48) Solomon, O. M., Jr. *PSD Computations Using Welch's Method. [Power Spectral Density (PSD)]*, 1991; p SAND-91-1533, 5688766. .
(49) Gao, X.; Lee, J.; White, H. S. Natural Convection at Microelectrodes. *Anal. Chem.* **1995**, *67* (9), 1541−1545.
(50) Amatore, C.; Pebay, C.; Thouin, L.; Wang, A.; Warkocz, J.-S. Difference between Ultramicroelectrodes and Microelectrodes: Influence of Natural Convection. *Anal. Chem.* **2010**, *82* (16), 6933−6939.
(51) Francke, R.; Little, R. D. Redox Catalysis in Organic Electrosynthesis: Basic Principles and Recent Developments. *Chem. Soc. Rev.* **2014**, *43* (8), 2492.
(52) Compton, R. G.; Banks, C. E. *Understanding Voltammetry*, 3rd ed.; World Scientific (Europe): 2018. DOI: 10.1142/q0155.
(53) Denuault, G.; Fleischmann, M.; Pletcher, D.; Tutty, O. R. Development of the Theory for the Interpretation of Steady State Limiting Currents at a Microelectrode. *J. Electroanal. Chem. Interfacial Electrochem.* **1990**, *280* (2), 243−254.
(54) Fan, B.; Wolfrum, B.; Robinson, J. T. Impedance Scaling for Gold and Platinum Microelectrodes. *J. Neural Eng.* **2021**, *18* (5), 056025.
(55) Pajkossy, T.; Jurczakowski, R. Electrochemical Impedance Spectroscopy in Interfacial Studies. *Curr. Opin. Electrochem.* **2017**, *1* (1), 53−58.
(56) Gabrielli, C.; Keddam, M.; Portail, N.; Rousseau, P.; Takenouti, H.; Vivier, V. Electrochemical Impedance Spectroscopy Investigations of a Microelectrode Behavior in a Thin-Layer Cell: Experimental and Theoretical Studies. *J. Phys. Chem. B* **2006**, *110* (41), 20478−20485.
(57) Roehrich, B.; Liu, E. Z.; Silverstein, R.; Sepunaru, L. Detection and Characterization of Single Particles by Electrochemical Impedance Spectroscopy. *J. Phys. Chem. Lett.* **2021**, *12* (40), 9748−9753.
(58) Balabajew, M.; Roling, B. Minimizing Artifacts in Three-Electrode Double Layer Capacitance Measurements Caused by Stray Capacitances. *Electrochimica Acta* **2015**, *176*, 907−918.
(59) Bewick, A.; Bewick, A.; Fleischmann, M.; Liler, M. Some Factors in Potentiostat Design. *Electrochimica Acta* **1959**, *1* (1), 83−105.
(60) Johnson, J. F. Hybrid Infrared Focal Plane Signal and Noise Model. *IEEE Trans. Electron Devices* **1999**, *46* (1), 96−108.
(61) Sarpeshkar, R.; Delbruck, T.; Mead, C. A. White Noise in MOS Transistors and Resistors. *IEEE Circuits Devices Mag.* **1993**, *9* (6), 23−29.
(62) Murmann, B. Thermal Noise in Track-and-Hold Circuits: Analysis and Simulation Techniques. *IEEE Solid-State Circuits Mag.* **2012**, *4* (2), 46−54.
(63) Warburg, E. Ueber Das Verhalten Sogenannter Unpolarisirbarer Elektroden Gegen Wechselstrom. *Ann. Phys.* **1899**, *303* (3), 493−499.
(64) Muralidharan, V. S. Warburg Impedance - Basics Revisited. *Anti-Corros. Methods Mater.* **1997**, *44* (1), 26−29.
(65) Abrantes, L. M.; Fleischmann, M.; Peter, L. M.; Pons, S.; Scharifker, B. R. On the Diffusional Impedance of Microdisc Electrodes. *J. Electroanal. Chem. Interfacial Electrochem.* **1988**, *256* (1), 229−233.
(66) Xie, Z.; Holdcroft, S. Polarization-Dependent Mass Transport Parameters for Orr in Perfluorosulfonic Acid Ionomer Membranes: An EIS Study Using Microelectrodes. *J. Electroanal. Chem.* **2004**, *568*, 247−260.